Supplementary Material: Effects of LGM sea surface temperature and sea ice extent on the isotope-temperature slope at polar ice core sites

Alexandre CAUQUOIN[1], Ayako ABE-OUCHI[2], Takashi OBASE[2], Wing-Le CHAN[3], André PAUL[4] and Martin WERNER[5]

[1]Institute of Industrial Science (IIS), The University of Tokyo, Kashiwa, Japan
[2]Atmosphere and Ocean Research Institute (AORI), The University of Tokyo, Kashiwa, Japan
[3]Research Center for Environmental Modeling and Application, Japan Agency for Marine-Earth Science and Technology (JAMSTEC), Yokohama, Japan
[4]MARUM – Center for Marine Environmental Sciences and Department of Geosciences, University of Bremen, Bremen, Germany
[5]Alfred Wegener Institute (AWI), Helmholtz Centre for Polar and Marine Sciences, Bremerhaven, Germany

Correspondence to: Alexandre Cauquoin (cauquoin@iis.u-tokyo.ac.jp)

Supplementary text: ECHAM6-wiso sensitivity simulations

Several sets of LGM and PI sensitivity simulations with ECHAM6-wiso have been performed:

- The maps of LGM-PI anomalies in 2m air temperature, precipitation and $\delta^{18}O_p$ according to our different ECHAM6-wiso are displayed in Figure S1, S2 and S3, respectively. The Figure S5 shows the model-data comparison of $\Delta_{LGM\text{-}PI}\delta^{18}O_{sn}$ at polar ice core stations for the strong LGM AMOC case. The average modeled values of $\delta^{18}O_p$-temperature temporal slope for East Antarctic, West Antarctic and Greenland regions according to our different simulations are indicated in Figure S6.

- In ECHAM6-wiso, the isotopic composition of sea ice surfaces also reflects the isotopic composition of snow (PI $\delta^{18}O$ between -5 and -30 ‰) deposited on this surface (Bonne et al., 2019; Cauquoin and Werner, 2021), meaning that sublimation of deposited snow on sea ice influences the isotopic composition of the above surface water vapor. This process leads to a stronger depletion of surface water vapor over sea ice covered areas. We disabled this process in LGM and PI simulations using MIROC 4m SST and sea ice (i.e., LGM_miroc4m_sst_and_sic and the corresponding PI simulations). In this case, the isotopic composition of sea ice surfaces equals the one of the ocean waters just beneath the sea ice, only (i.e., $\delta^{18}O$ around 0 ‰). The impacts on modeled $\delta^{18}O_p$-temperature temporal slopes in polar regions are shown in Figure S7.

- The sea ice area fraction from MIROC 4m is lower in coastal grid cells (see section 2.2.2), especially in the Arctic. To evaluate the impacts of this parameterization on modeled $\delta^{18}O_p$-temperature temporal slopes, LGM and PI sea ice fields from MIROC 4m (from LGM_miroc4m_sst_and_sic and the corresponding PI simulations, see Table 1) are modified in the following way: (1) monthly sea ice area fraction cannot decrease going north (south) in the Northern (Southern) Hemisphere and (2) all monthly sea ice area fraction values above 95 % are set to 100 ‰ (Figure S8). The impacts on modeled $\delta^{18}O_p$-temperature temporal slopes in Greenland region are shown in Figure S9.

- To test if the general bias in modeled $\delta^{18}O$ in Antarctica is due to the GLAC-1D LGM ice sheet reconstruction prescribed for the ECHAM6-wiso simulation, another LGM simulation using the PMIP3 ice sheet reconstruction instead of GLAC-1D has been performed. The PMIP3 ice sheet reconstruction contains stronger elevation changes in Antarctica, especially in the western part of the continent (see Figure 3 of Werner et al., 2018). We used the sea surface boundary conditions from GLOMAP for this simulation. The model-data comparison and the spatial distribution of modeled $\delta^{18}O_p$-temperature temporal slope in Antarctic and Greenland areas are shown in Figure S4 and S10, respectively.

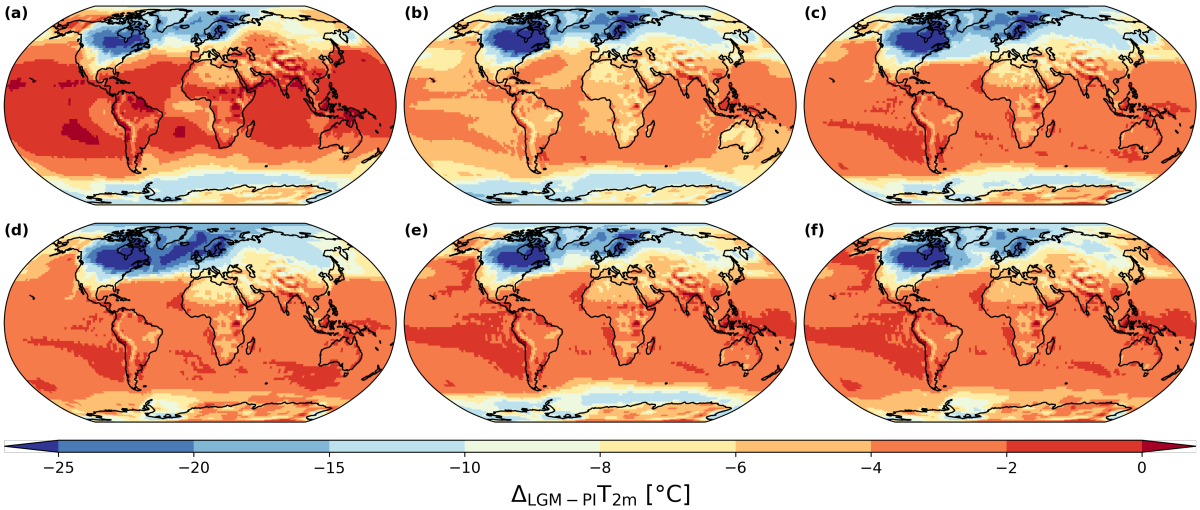

Figure S1: Modeled 2m air temperature anomalies between LGM and PI from our different ECHAM6-wiso simulations: (a) LGM_GLOMAP, (b) LGM_tierney2020, (c) LGM_miroc4m_sst_glomap_sic, (d) LGM_miroc4m_sst_and_sic, (e) LGM_miroc4m_strong_AMOC_sst_glomap_sic, and (f) LGM_miroc4m_strong_AMOC_sst_and_sic.

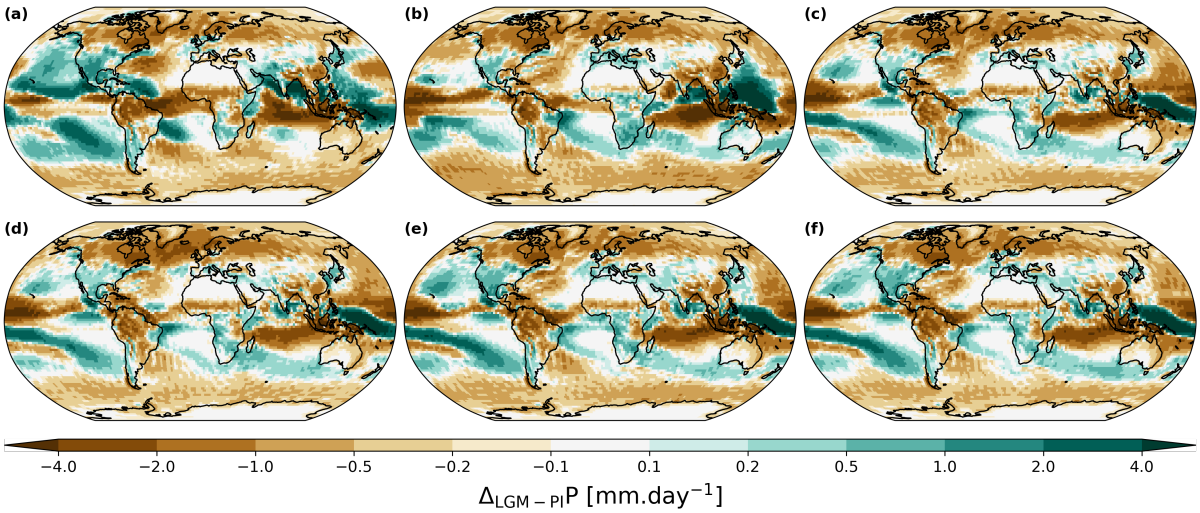

Figure S2: Same as Figure S1 but for modeled precipitation anomalies.

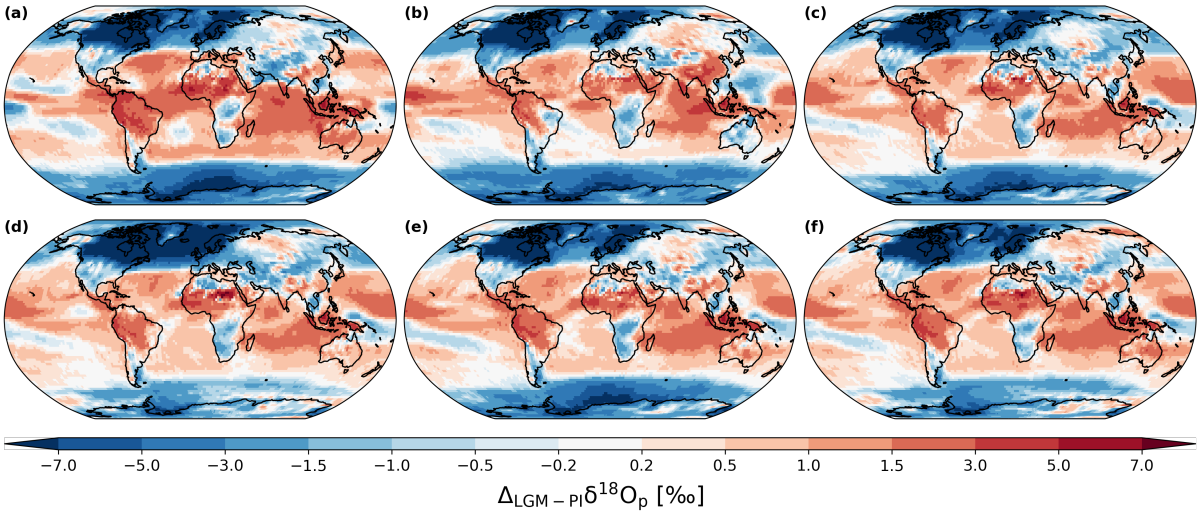

Figure S3: Same as Figure S1 but for modeled $\delta^{18}O_p$ anomalies.

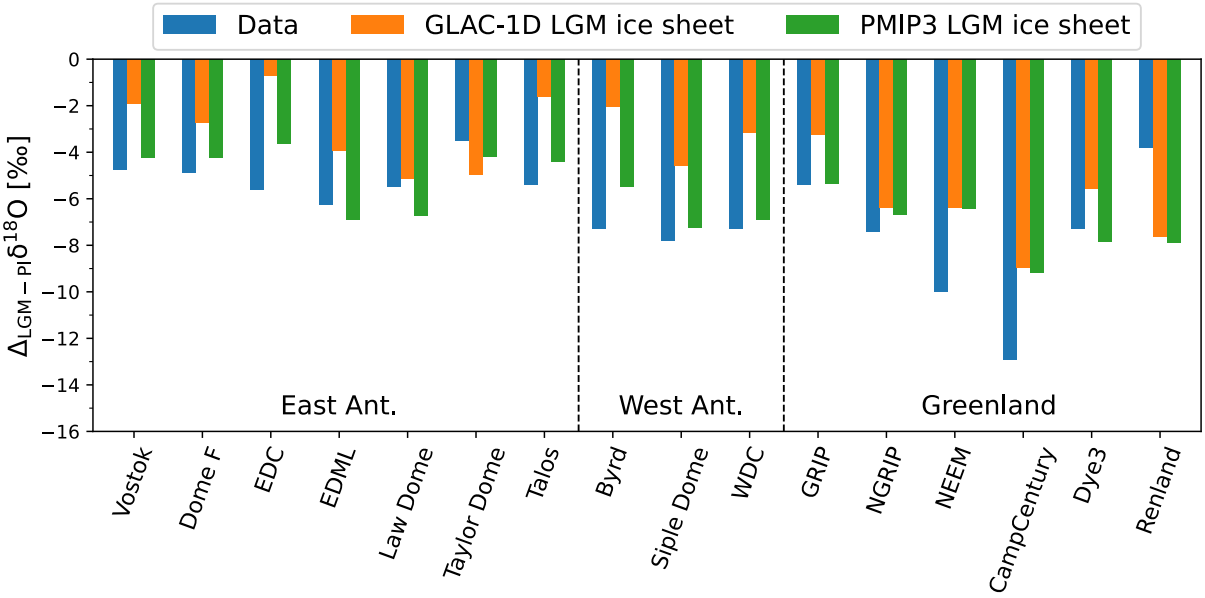

Figure S4: Comparison of $\delta^{18}O$ anomalies measured in polar ice cores (blue bars) with modeled anomalies in $\delta^{18}O_{sn}$ between LGM and PI from ECHAM6-wiso simulations using the PMIP3 LGM ice sheet or GLAC-1D (green and orange bars, respectively). The sea surface boundary conditions are from GLOMAP for the two simulations.

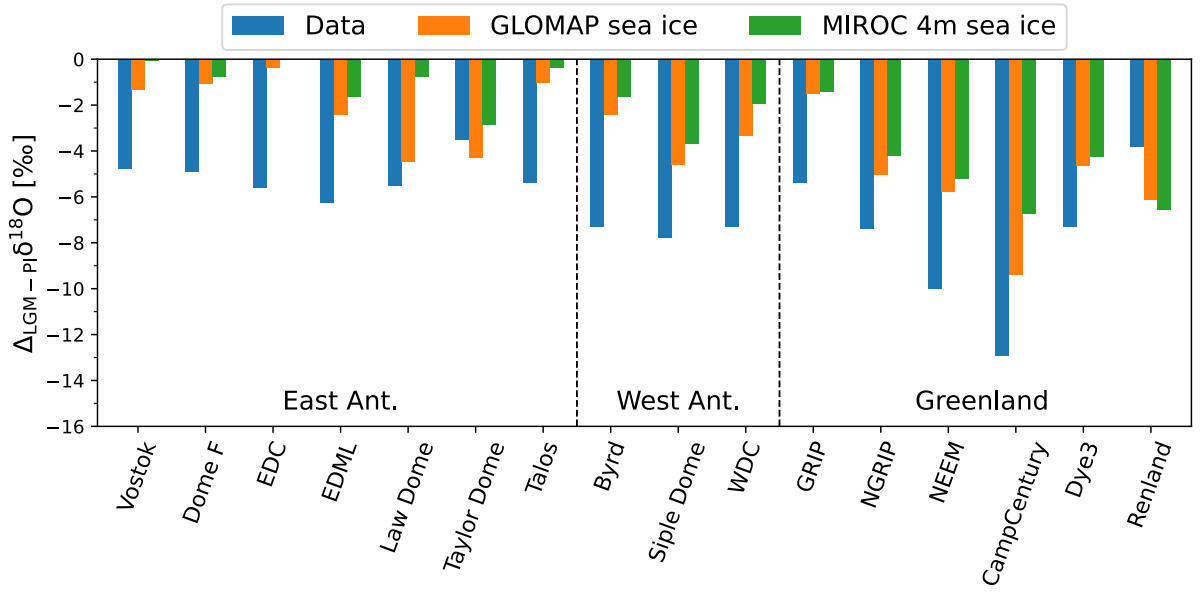

Figure S5: Same as Figure 6a but with SST (green and orange bars) and sea ice (green bars) from MIROC 4m with strong LGM AMOC simulation.

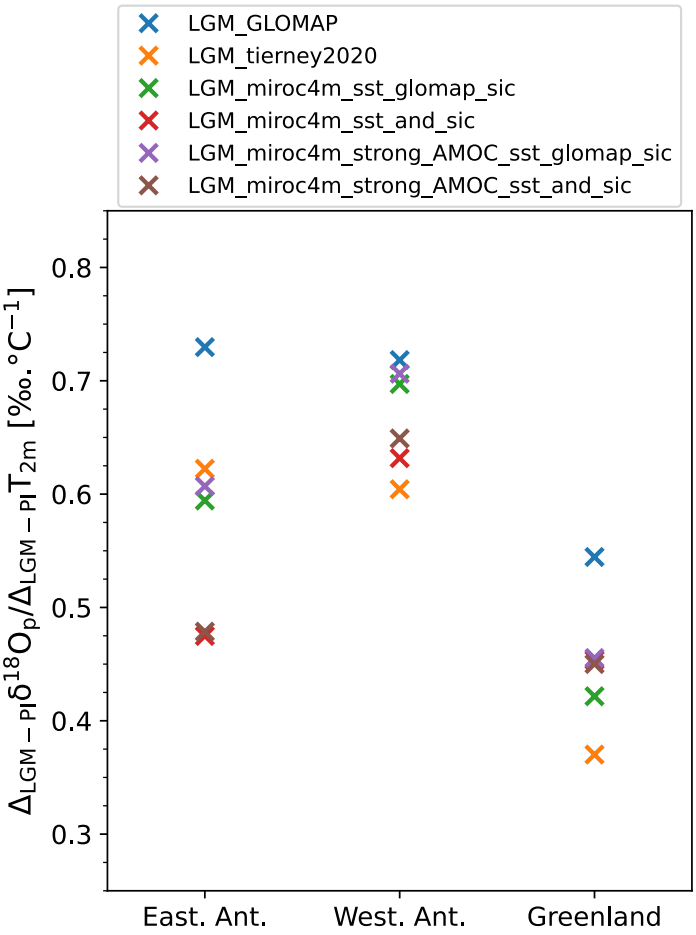

Figure S6: Average modeled values of $\delta^{18}O_p$-temperature temporal slope for East Antarctic, West Antarctic and Greenland regions according to our different simulations.

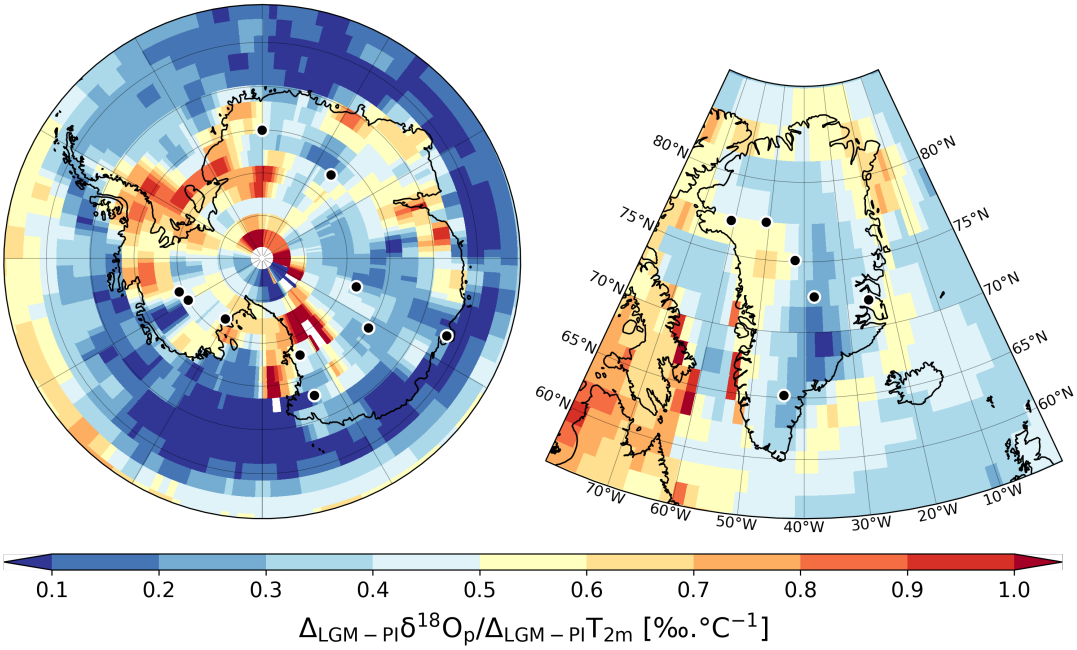

Figure S7: Spatial distribution of $\delta^{18}O_p$-temperature temporal slope in Antarctic and Greenland areas (left and right plots, respectively) for LGM-PI changes using the same sea surface boundary conditions as in LGM_miroc4m_sst_and_sic simulation, but without taking into account the isotopic content of snow on sea ice for sublimation processes in sea ice covered regions (see text at the beginning of this Supplementary Material).

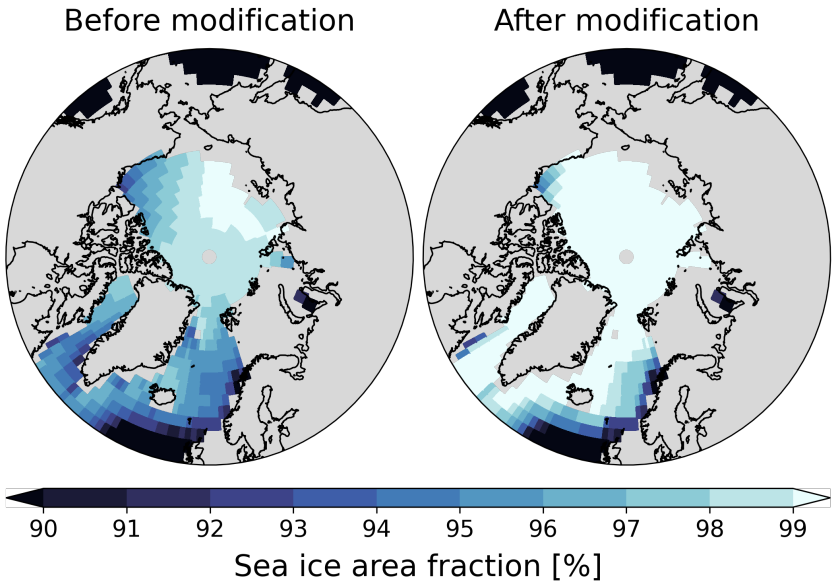

Figure S8: Mean LGM sea ice area fraction from MIROC 4m (LGM_miroc4m_sst_and_sic simulation) before and after the modifications described in the text at the beginning of this Supplementary Material.

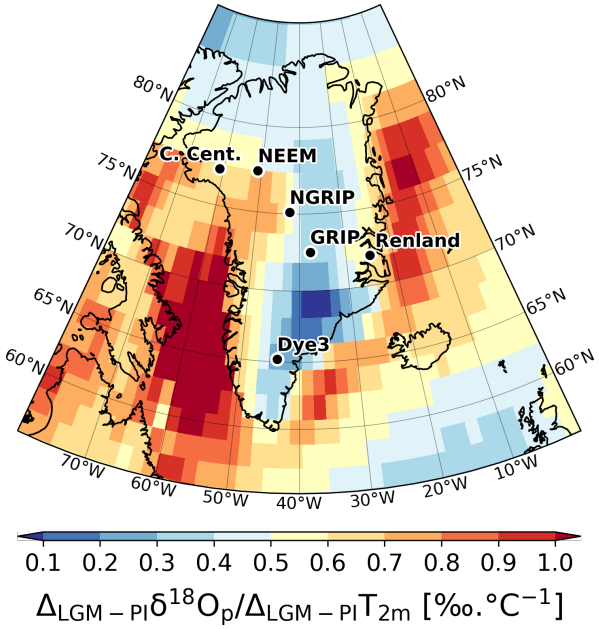

Figure S9: Spatial distribution of $\delta^{18}O_p$-temperature temporal slope in Greenland area for LGM-PI changes using the modified sea ice field boundary conditions shown in Figure S8 (see text at the beginning of this Supplementary Material for details).

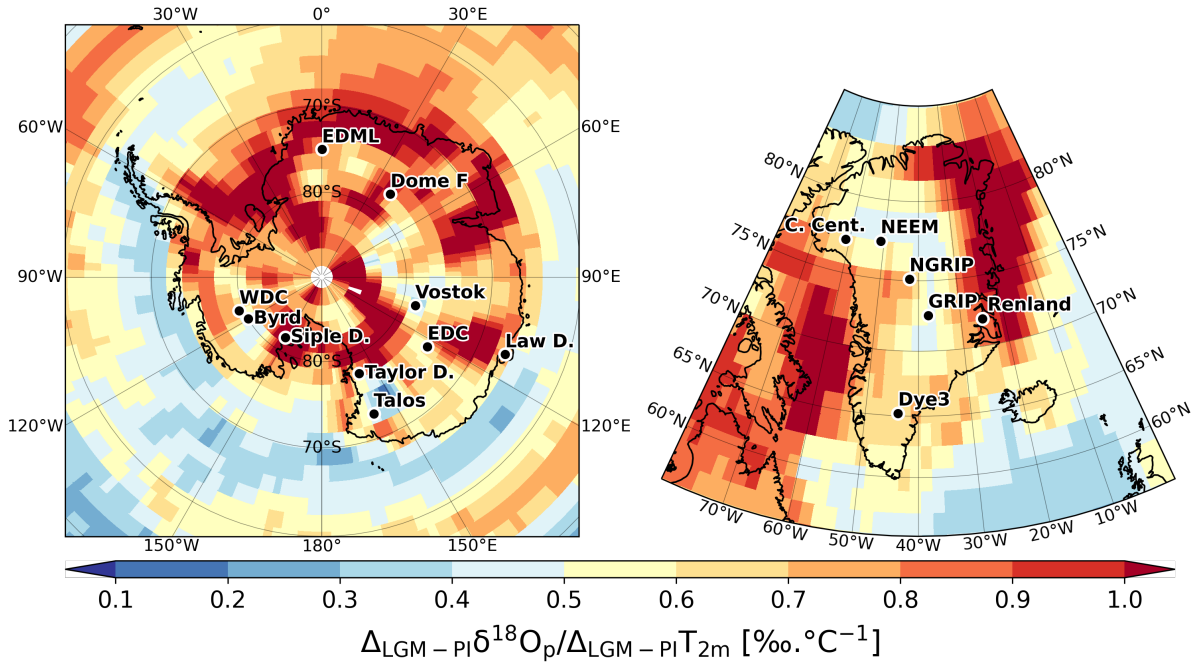

Figure S10: Spatial distribution of $\delta^{18}O_p$-temperature temporal slope in Antarctic and Greenland areas (left and right plots, respectively) for LGM-PI changes using the PMIP3 LGM ice sheet reconstruction instead of GLAC-1D.

References

Bonne, J.-L., Behrens, M., Meyer, H., Kipfstuhl, S., Rabe, B., Schönicke, L., Steen-Larsen, H. C., and Werner, M.: Resolving the controls of water vapour isotopes in the Atlantic sector, Nat. Commun., 10, 1632, https://doi.org/10.1038/s41467-019-09242-6, 2019.

Cauquoin, A. and Werner, M.: High-Resolution Nudged Isotope Modeling With ECHAM6-Wiso: Impacts of Updated Model Physics and ERA5 Reanalysis Data, J. Adv. Model. Earth Syst., 13, https://doi.org/10.1029/2021MS002532, 2021.

Werner, M., Jouzel, J., Masson-Delmotte, V., and Lohmann, G.: Reconciling glacial Antarctic water stable isotopes with ice sheet topography and the isotopic paleothermometer, Nat. Commun., 9, https://doi.org/10.1038/s41467-018-05430-y, 2018.